Available online at www.sciencedirect.com
SCIENCE DIRECT®
Journal of Solid State Chemistry 172 (2003) 102–110
JOURNAL OF SOLID STATE CHEMISTRY
http://elsevier.com/locate/jssc

A novel ultrasound-assisted approach to the synthesis of CdSe and CdS nanoparticles

Hong-liang Li, Ying-chun Zhu, Si-guang Chen, Oleg Palchik, Jin-ping Xiong, Yuri Koltypin, Yosef Gofer, and Aharon Gedanken*

Department of chemistry, Bar-Ilan University, Ramat-Gan 52900, Israel

Received 21 August 2002; received in revised form 22 October 2002

Abstract

Hexagonal CdSe and hexagonal CdS nanoparticles have been prepared using $Cd(Ac)_2$ and less hazardous elemental Se or S as precursors, respectively, with the aid of ultrasound irradiation under an atmosphere of H_2/Ar (5/95, V/V). The products consist of 7–10 nm nanocrystallites which aggregated in the form of polydispersive nanoclusters with sizes in the range 30–40 nm in the case of CdSe, and near monodispersive nanoclusters with a mean size of about 40 nm in the case of CdS. X-ray diffraction, high-resolution TEM and SAED patterns (selected area electron diffraction patterns) show that the as-prepared particles are well crystallized. X-ray photoelectron spectroscopy (XPS) measurements further confirm the formation of CdSe and CdS. Diffuse reflection spectra indicate that both the CdSe and the CdS nanocryslallites are direct band-gap semiconductors with band-gap values of about 1.83 and 2.62 eV, respectively. Control experiments demonstrate that the hydrogen is the reducing agent, and the extreme high temperature induced by the collapse of the bubble accelerates the reduction of elemental Se or S by hydrogen. An ultrasound assisted in situ reduction/combination mechanism is proposed.

Keywords: Ultrasound; CdSe; CdS; Nanoparticles; XRD; TEM; DRS; XPS

1. Introduction

Nanoparticles are the subject of considerable interest in many different scientific disciplines [1–6]. This interest derives from the various special properties of materials in the nanoscale regime, including (photo) catalytic [7], mechanical [8], electrical and optical [9,10]. Semiconductor nanoparticles usually exhibit variable and often controllable properties, in particular for the change of energy structure (including band gap), and enhanced surface properties with decrease in size which affect all their optoelectronic properties [11]. Semiconductor selenides and sulfides have already found application as sensors or laser materials [12], optical filters [13], solar cells [14], and in many other devices [15–17]. Therefore, the synthesis of binary metal chacogenides semiconductors has received intense attention recently due to their important physical and chemical properties. Many approaches have been suggested for the synthesis of group II–VI semiconductor crystallites or nanocrystallines, such as gas-phase reactions between the element or its compounds and gaseous H_2Se [18], solid-state reaction [19], chemical bath deposition [20], and pyrolysis of single source precursors [21]. Generally, all these reactions require high temperature (500°C), and the use of toxic and highly sensitive precursors.

An important landmark in the development of wet chemical routes for the synthesis of cadmium chalcogenide nanocrystals goes together with the nonaqueous TOP/TOPO (trioctylphoshine/trioctylphosphine oxide) technique [22], and the use of different thiols as stabilizing agents in aqueous solution [23–26]. A series of monodispersive thioalcohol-stabilized CdS and CdTe nanoparticles with extremely small sizes (1–3 nm size range) were synthesized in aqueous solution and obtained in the gram scale quantities. Yet, these methods need additives. Recently, Parkin et al. [27] reported a direct combination of elements in amine for the synthesis of metal chalcogenides. However, the obtained products ZnE and CdE (E = S, Se or Te) were X-ray amorphous and needed to be crystallized at above

*Corresponding author. Fax: +972-3-535-1250.
E-mail address: gedanken@mail.biu.ac.il (A. Gedanken).

0022-4596/03/$ - see front matter © 2002 Elsevier Science (USA). All rights reserved.
doi:10.1016/S0022-4596(02)00138-X

300°C. Bandaranayke et al. [28] reported a method for synthesis of Cd*E* crystallites using aqueous solution precipitation from Na_2E and $CdCl_2$ followed by thermal annealing at high temperature. Subsequently, a thermalsolvent method was studied [29] and many main groups and transient metal chalcogenides have been prepared through this method [30–33]. However, this method still needs relatively high temperature or high pressure and long reaction time (several hours to days). A room temperature method to the synthesis of Cd*E* nanoparticles using KBH_4 as reducing agent was also reported [34]. Very recently, high quality Cd*E* were prepared using CdO as precursor with the presence of hexylphosphonic acid (HPA) or tetradecylphoshonic acid (TDPA) in trioctylphosphine at about 300°C [35]. Our previous studies show that the microwave-assisted methods are also useful to the preparation of some metal selenides [36,37]. To get high-quality materials under mild conditions and using safe precursors at a relative low temperature has been the current issue of semiconductors synthesis. The sonochemical method has been used extensively to generate novel materials [38–41]. Its chemical effects have recently come under investigation for the acceleration of chemical reaction [42,43] and for the synthesis of new materials with unusual properties [44,45]. A sonoelectrochemical method to produce cubic phase CdSe nanocrystals [46] and PbSe nanoparticles [47] and a general sonochemical method to give ZnSe nanoparticles [48] had been developed in our group. In this paper, we report on a new sonochemical approach to metal chalcogenides. Comparing with that of the previously studied sonochemical method, the new method is much simpler, safe, and more general for the preparation of metal chalcogenides nanoparticles. Furthermore, it has a different reaction mechanism, which leads to crystallized product and to different phase for CdSe.

2. Experimental section

$Cd(Ac)_2$, elemental S, Se powder (~100 mesh) and dimethyl sulfoxide (DMSO) were purchased from Aldrich and were used without further purification. Ultrasonic irradiation was achieved with a high-intensity ultrasonic probe (Misonix; XL sonifier, 1.13 cm diameter Ti horn, 20HZ, 60 Wcm^{-1}). The X-ray diffraction (XRD) patterns were recorded on a Rigaku X-ray diffractometer (model-2028, Co$K\alpha$ $\lambda = 1.78892$ Å). Morphology and structure investigations were performed with a JEOL-JEM 100SX transmission electron microscopy (TEM) with 100 kV accelerating voltage. High-resolution TEM (HRTEM) images were taken using a JEOL-3010 with 300 kV accelerating voltage. A conventional monochrome CCD camera, with resolution of 768 × 512 pixels, was used to digitize the images. The digital images were processed with the digital micrograph software package (Gatan, Inc, Pleasanton, CA, USA). The X-ray photoelectron spectroscopy (XPS) data were accumulated on an AXIS HS (Kratos analytical) electron spectrometer system with monochromatized Al Kα standard X-ray source. The binding energies were calibrated by referencing the C1 s to 285.0 eV. UV–Vis diffuse reflectance spectrophotoscopy (DRS) were measured by a Cary 500 UV–Visible spectrophotometer at room temperature.

In a typical procedure, 0.700 g $Cd(Ac)_2 2H_2O$ and 0.200 g elemental Se (or 0.082 g S) were dispersed in 80 ml DMSO, and the mixture was irradiated with high-intensity ultrasound radiation for 3 h under H_2/Ar (5/95, V/V) atmosphere at room temperature. During irradiation, the color of the suspension changed and the temperature rose to 130°C. After irradiation, the resulting suspension was cooled to room temperature and then centrifuged, and the precipitate was washed twice with absolute ethanol and water, respectively. The solid was dried in vacuum at room temperature for 6 h. To understand the mechanism of the reaction, control experiments, such as irradiating the mixture of the precursors under pure Ar atmosphere or by heating the mixture under H_2/Ar atmosphere instead of using ultrasound irradiation, have been carried out.

3. Results and discussion

3.1. XRD studies

Fig. 1 presents the XRD patterns of the as-prepared solids. The solids corresponding to curves A and B can be attributed to hexagonal CdSe (JCPDS file No. 8-459) and hexagonal CdS (JCPDS file No. 6-314), respectively. The peaks are broadened, showing that the size of the particles is small [49]. Comparing with the previously developed sonoelectrochemical method [46] and the general microwave method [36], which obtained the cubic phase CdSe nanoparticles, the present method got a hexagonal phase of CdSe.

To obtain more quantitative information, Debye–Scherrer formula [50]

$$L = 0.9\lambda/(B \times \cos(\theta)) \quad (1)$$

has been applied to calculate the size of the nanocrystals. Where L is the coherence length, B is the full-width at half-maximum (fwhm) of the peak, λ is the wavelength of the X-ray radiation, and θ is the angle of diffraction. In the case of spherical crystallites, the relation between L and D, the diameter of the crystallite, is given by $L = \frac{3}{4}D$. The values of L obtained for CdSe and CdS are 8.1 and 6.8 nm, respectively. This translates to a crystallite size of 10.8 and 9.1 nm, respectively.

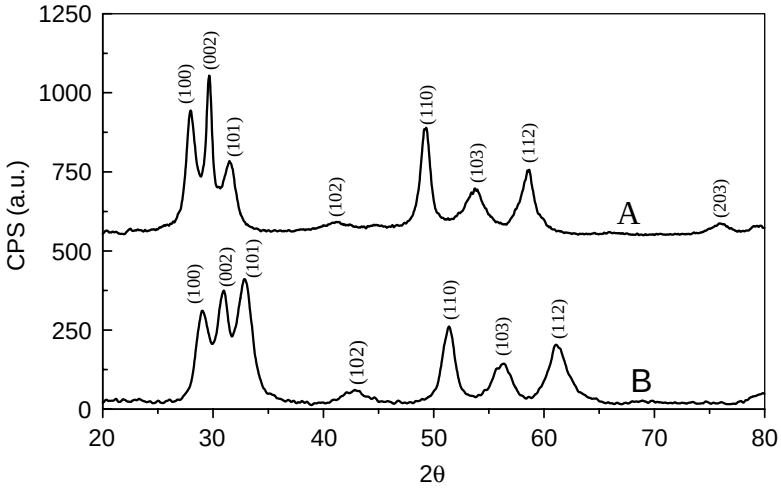

Fig. 1. XRD patterns of the as-prepared samples: (A) for CdSe; (B) for CdS.

3.2. TEM and high-resolution TEM

The morphologies of the as-prepared CdSe and CdS were characterized by transmission electron microscopy (TEM), and the images and the corresponding SAED are shown in Figs. 2(A, B) and (C, D), respectively. From picture A we can see that the CdSe nanoparticles are aggregated into nanoclusters with sizes of about 30–40 nm. Its SAED shows a spotty pattern (Fig. 2B), which means that the as-prepared particles were well crystallized. The diffraction spots can be indexed to the (100), (002), (110) and (112) planes, confirming the formation of hexagonal CdSe. Picture C is the TEM image of the as-prepared CdS, which shows near monodispersive spherical nanoclusters with a mean diameter of about 40 nm, which also consist of little nanoparticles. The selected area diffraction pattern shows observable rings (Fig. 2D), which means the particles are polycrystalline. The indexing of the diffraction rings of SAED pattern confirms the (100), (002), (101), (110), (103) and (112) planes of the wurtzite phase of CdS.

In order to further elucidate the size and the crystal structure of the nanoparticles that compose the clusters, HRTEM images were taken. Figs. 3A and B show the HRTEM of CdSe nanoparticles in different magnifications. An overview image (A) shows the individual nanoparticle with size of about 7–10 nm. It is near to the size derived from the Debye–Scherrer formula. In the large magnification image (B), the lattice fringes are clearly visible, confirming their crystallinity. The observed lattice space of 3.28 Å corresponds to the (1 0 1) plane of hexagonal CdSe [51]. Figs. 3C and D show the HRTEM images of CdS. From the overview image (C) we can see the individual CdS nanoparticles with size of about 5–8 nm. The large magnification image (D) show very observable lattice fringes. A lattice space with value of about 3.18 Å was calculated, which is corresponding to the (101) plane of hexagonal CdS [52]. As is shown in image B and D, some stacking faults are present for both CdSe and CdS nanoparticles, which have also been observed previously in CdSe nanoparticles prepared by other methods [22,53].

3.3. XPS results

X-ray photoelectron spectroscopy (XPS) has been used to derive the composition information of the as-prepared particles. High-resolution spectra have been taken in Cd3*d* and Se3*d* regions for CdSe (Figs. 4(a) and (b)) and Cd3*d* and S2*p* regions for CdS (Figs. 4(c) and (d)), respectively. From Figs. 4(a) and (b) we can see that the Cd3*d* core shows two peaks at 405.7 and 412.4 eV, respectively, and Se3*d* survey shows one broad peak at about 54 eV. This latter peak can be deconvoluted by Gaussian–Lorenzian functions to two peaks with peak positions at 54.4 and 54.8 eV, respectively, which correspond well with the characteristic Se3*d* core levels of CdSe crystal [54,55]. Quantification of the XPS peaks intensities gives the ratio of Cd/Se as 0.983, which is consistent with the stoichiometry of CdSe. From Figs. 4(c) and (d) we can see that there are two peaks at 161.7 and 405.1 eV corresponding to S2*p* and Cd3*d* core levels of CdS, respectively, which are very consistent with previously reported results [56]. The quantification of the peaks gives a Cd-to-S ratio of 1.07:1. For both CdSe and CdS, and no peaks corresponding to CdO are observed. In the Se case, no SeO_2 signal appears at about 59 eV [55]. The XPS results further confirm the formation of CdSe and CdS.

3.4. Optical properties

We have measured the diffusion reflection spectra (DRS) of the as-prepared CdSe crystals and CdS nanoparticles in order to understand their excitonic or

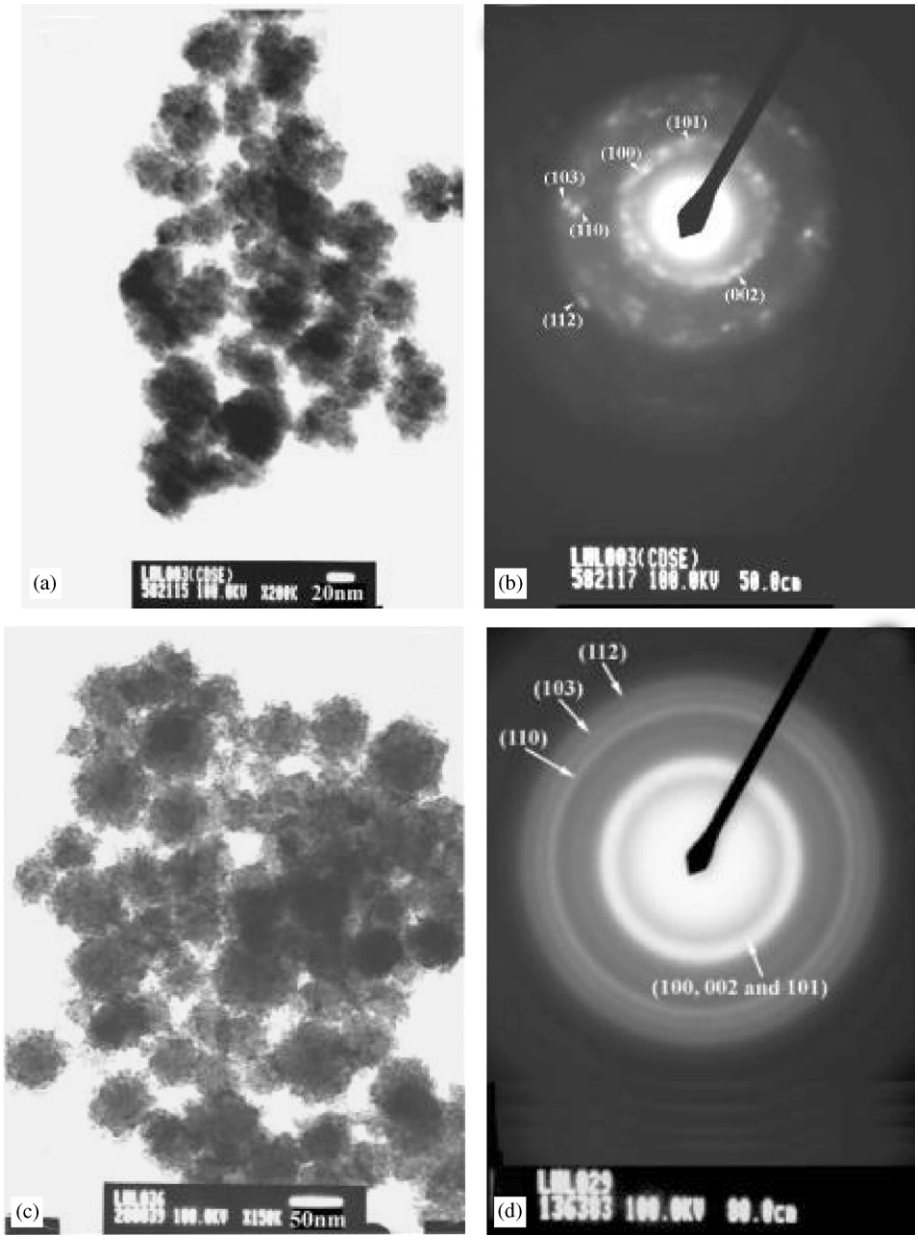

Fig. 2. TEM images and the corresponded SAED patterns of the as-prepared solids: (A) and (B), CdSe; (C) and (D), CdS.

interband (valence conduction band) transitions, which allow us to calculate their band gap.

Figs. 5(a) and (b) depict the diffuse reflection spectra of the as-prepared CdSe and CdS nanoparticles, respectively. Both curves show steep slopes, which indicate the size of the particles is near monodispersive. An estimate of the optical band-gaps is obtained using the following equations [57]:

$$\alpha(v) = A(h'v - Eg)^{m/2}, \quad (2)$$

Where $h' = h/2\pi$, $h'\nu$ is the photon energy, α is the absorption coefficient, while m is dependent on the nature of the transition. For a direct transition m is equal to 1 or 3, while for an indirect allowed transition m is equal to 4 or 6. Since α is proportional to $F(R)$, the Kubelka–Munk function $F(R) = (1-R)^2/2/R$, the energy intercept of a plot of $(F(R) \times hv)^2$ versus hv gives Eg for a direct allowed transition when the linear region is extrapolated to the zero ordinate. Using this method, the band gaps of the CdSe and CdS nanoparticles have been obtained to be 1.83 and 2.60 eV, respectively. Figs. 5(c) and (d) give the normalized plots deriving from the calculated data of curves (a) and (b), respectively. Similar results are obtained if $(F(R) \times hv)^{1/2}$ is plotted against hv as is appropriate for an indirect semiconductor. For the present comparative exercise, however, we have opted to use the equation for a direct semiconductor in accordance with common

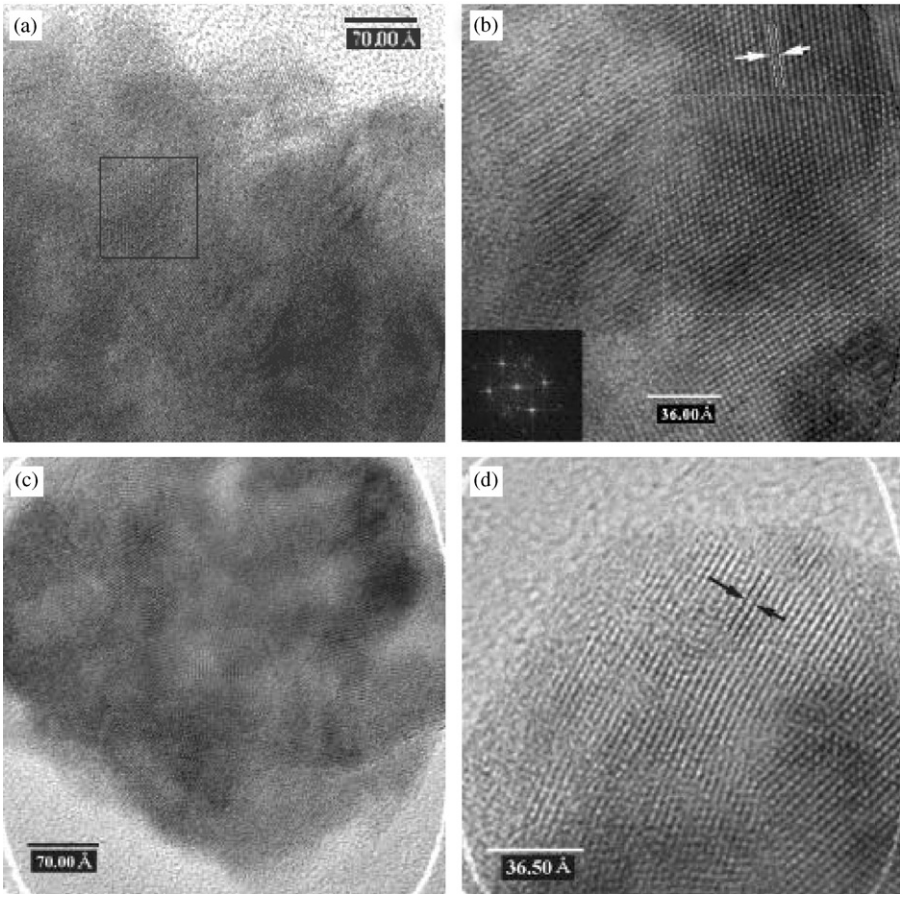

Fig. 3. HRTEM images: (A) overview of CdSe; (B) high magnification of CdSe (the inset is the fast Fourier transform (FFT) of the selected area; (C), overview of CdS; (D) high magnification of CdS.

practice [57–59]. A band gap of 1.83 eV is obtained, which is larger than that of the bulk crystalline CdSe (the room temperature bulk band gaps for hexagonal CdSe and cubic CdSe are 1.73 [37] and 1.74 eV [58], respectively). Our calculated band gap fit previous values obtained for particle size between 5.5 and 8 nm where the corresponding band gaps are 1.90 and 1.73 eV, respectively [46]. A value of 2.60 eV is also higher than that of the bulk CdS crystal (the band gap of bulk CdS crystal is 2.42 eV). A similar blue shift had also been observed in CdS films, which consist of CdS grains with size value between several to tens nanometers [59–61]. Their band gap also varied between 2.4 and 2.6 eV.The blue shift can be attributed to the quantization effect of the nanoscale particles [62,63].

3.5. Proposed reaction mechanism

In order to understand the mechanism of the reaction, some control experiments have been conducted. For example, the original mixture of the precursors was sonicated in a pure Ar atmosphere. Another control experiment was done by heating the same precursor mixture under an atmosphere of H_2/Ar instead of ultrasound irradiation. The roles of hydrogen gas and ultrasound radiation in the formation of CdSe are examined in this way. Fig. 6 gives the XRD results of these control experiments as compared with the XRD patterns of reactant Se (curve C) and of the as-prepared CdSe (curve D). When the reaction was carried out under a pure Ar atmosphere, no CdSe is formed (curve A); when the mixture was just heated at 140°C for 3 h without ultrasound, the solid obtained was identified as the reactant Se and in addition a small amount of CdSe (curve B). These control experiments show that the presence of hydrogen is essential to the formation of CdSe, and the ultrasound radiation can accelerate the reaction of the formation of CdSe.

It is known that there are three regions in the neighborhood of the collapsing bubbles: the gas phase inside the bubbles (where the temperature can reach 5000 K); the transient layer of the bubble (with a width of about 200 nm and a temperature of about 2000 K) and the bulk of the solvent [64,65]. The high temperatures and pressures produced in imploding cavitation bubbles lead to the thermal decomposition of water vapor or organic solvent vapor, forming radicals.

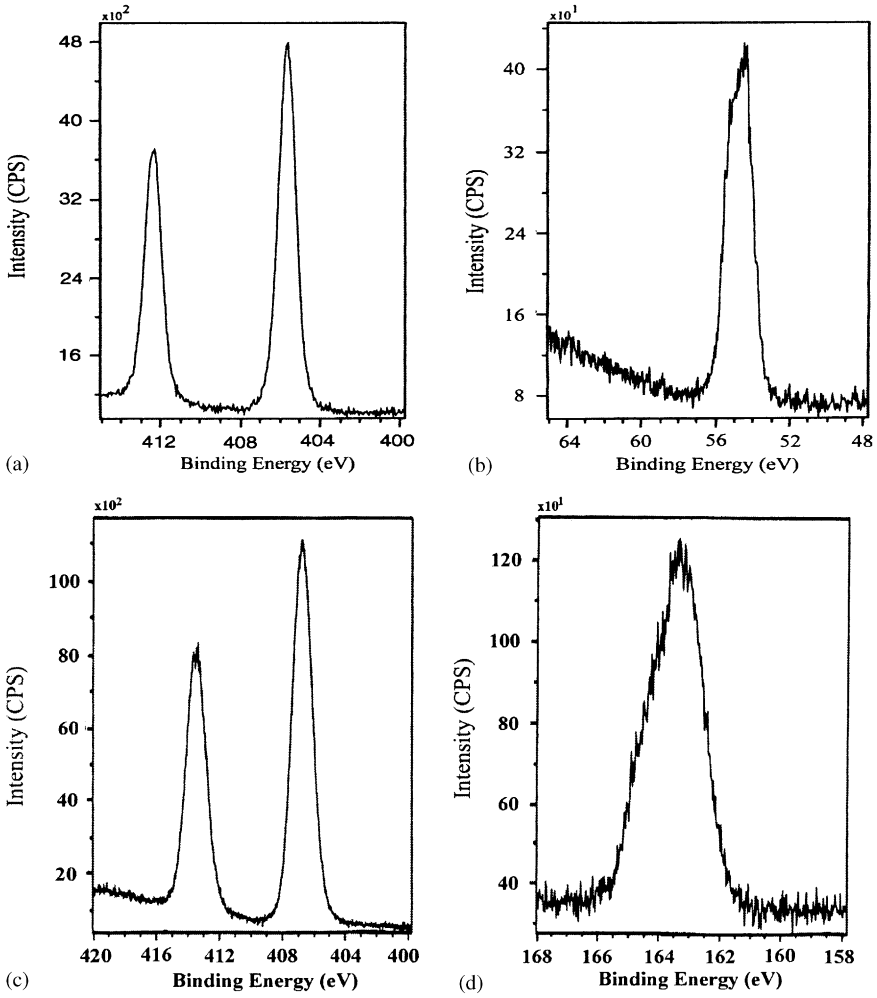

Fig. 4. High-resolution XPS surveys in Cd3*d* and Se3*d* regions for CdSe ((a) and (b)) and in Cd3*d* and S2*p* regions for CdS ((c) and (d)).

The mechanism of the formation of CdE (E=Se, S) takes into consideration the radical species obtained from the solvent DMSO [66] and from the water molecules [67] released from $Cd(Ac)_2 2H_2O$ precursor by absorption of untrasound [Eqs. (3) and (3′)].

$$DMSO \rightarrow {}^{\bullet}CH_3SO + {}^{\bullet}CH_3, \quad (3)$$

$$\mathbf{H_2O \rightarrow {}^{\bullet}H + {}^{\bullet}HO}. \quad (3')$$

The formed radicals in Eqs. (3) and (3′) can act as inducers and trigger the decomposition of excited $^{*}H_2$ molecule to $H^{\cdot}$ [Eqns. (4) and (4′)].

$${}^{\bullet}CH_3 + {}^{*}H_2 \rightarrow CH_4 + H^{\bullet}, \quad (4)$$

$${}^{\bullet}HO + {}^{*}H_2 \rightarrow H_2O + H^{\bullet}. \quad (4')$$

The $H^{\bullet}$ react with Se (or S) in the high-temperature interface region of the bubbles forming H_2Se (or H_2S) [Eq. (5)].

$$E + 2H^{\bullet} \rightarrow H_2E (E = Se, S). \quad (5)$$

The formed H_2E then reacts with Cd^{2+} to form CdE.

$$H_2E + Cd^{2+} \rightarrow CdE + 2H^{+}. \quad (6)$$

A nanocrystalline product would be expected if the reaction takes place at the interface [68]. On the other hand, an amorphous product would be obtained if the reaction takes place inside the bubble as a result of the high cooling rates ($>10^{10}$ K s^{-1}) which occur during the collapse [69]. Thus, the fact that crystalline products are obtained implies that Eq. (6) reaction takes place at the interface. A challenge to this mechanism is whether Cd^{2+} can be reduced to elemental Cd at Eq. (5) step. A control experiment shows that no elemental Cd is produced when $Cd(Ac)_2$ was dissolved in DMSO and irradiated by intense ultrasound under H_2/Ar atmosphere. This can be explained as due to the coordination of DMSO to Cd^{2+} forming complex and reducing the Cd^{2+}/Cd potential [70, 71]. Further evidence is that extending our synthetic method to CdTe has failed because of the more negative half-cell potential of

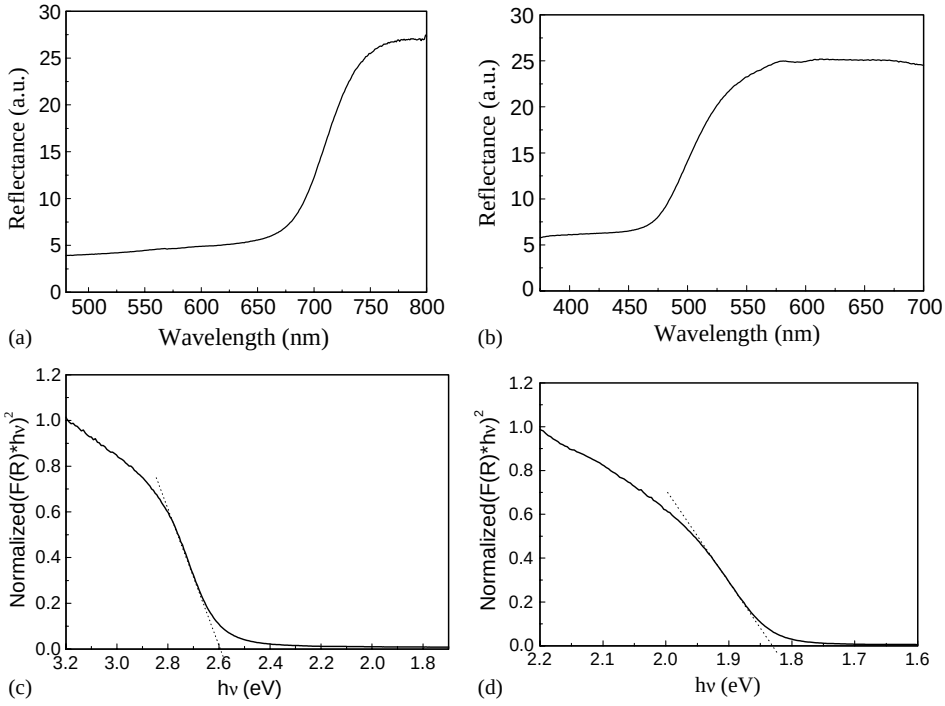

Fig. 5. Diffraction reflection spectra of the as-prepared CdSe (a) and CdS (b), and the normalized plots derived from the calculated data of them ((c), CdSe; (d), CdS).

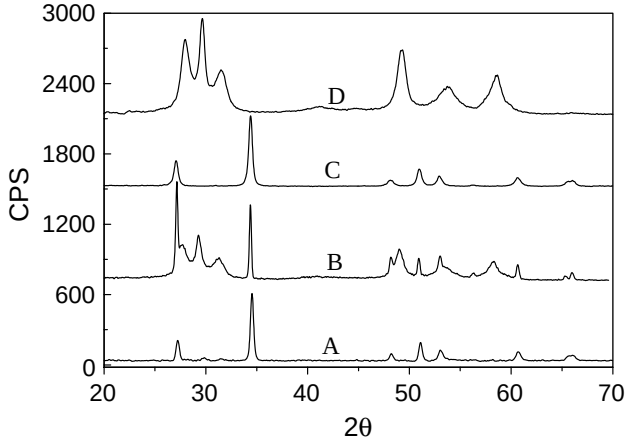

Fig. 6. XRD results of the control experiments and that of reactant Se and the as-prepared CdSe: (A) solid obtained by irradiating $Cd(Ac)_2$ and Se in DMSO under a pure Ar atmosphere; (B) solid resulting by heating $Cd(Ac)_2$ and Se in DMSO under a H_2/Ar atmosphere; (C) reactant Se; (D), as-prepared CdSe.

Te/Te^{2-} (−1.143 eV [72]). These reasons make us prefer the reduction of Se or S, which happens in Eq. (5) step. Another challenge to the mechanism is whether H_2 can decompose directly by absorption ultrasound in the interior forming $H^{\bullet}$ radicals. It has been shown that although the H_2 inside the bubble can be excited by ultrasound, most of the species still in molecular form and stay inside the bubbles [73], therefore, this possibility is also small.

4. Conclusion

An ultrasound-assisted sonochemistry reduction and then reaction in situ approach has been developed to prepare CdSe and CdS nanocrystallite using less hazardous Se (or S) and $Cd(Ac)_2$ as precursors in DMSO solvent. The as-prepared nanoparticles are well crystallized. Absorption bands in the visible region with a band gap value of about 1.83 eV for CdSe and a band gap value of about 2.60 eV for CdS were obtained, which are blue shifted compared with the band-gap value of the corresponded bulk crystal. An ultrasound induced reduction and then in situ combination mechanism have been proposed based on the extreme conditions produced by ultrasound irradiation. Compared with the previous reported method [46,47], the reaction mechanism is completely different. The current method does not need a chelating reagent, and the precursor materials of the reaction are safe. Using this method, other metal chacogenides nanocrystallite such as Cu*E* or Zn*E* (*E* = Se or S) can also be prepared.

Acknowledgments

Li H. L. thanks the Bar-Ilan Research Authority for a post-doctoral fellowship. Zhu Y. C. thanks the Kort 100 Scholarship Foundation for supporting his postdoctoral fellowships. Gedanken A. thanks the German Ministry of Science for the support of this work through the

Deutche-Israeli DIP program. The authors are grateful to Prof. Deutsch, M., Department of Physics and Mrs. Judy, Department of Life Science, for extending the use of their facilities to us. We thank Dr. Shifra Hochberg for editorial assistance. Kind assistance from Mrs. Avivi S., Dr. Kumar V. Ganesh, Mr. Pol Vilas G., Mr. Motiei Menachem and Mr. Grisaru Haviv is gratefully acknowledged.

References

[1] Y. Wang, N. Herron, J. Phys. Chem. 95 (1999) 525.
[2] H. Weller, Angew. Chem. Int. Ed. Engl. 32 (1993) 41.
[3] H. Weller, Adv. Mater. 5 (1993) 88.
[4] A.P. Alivisatos, J. Phys. Chem. 100 (1996) 13226.
[5] D.L. Klein, R. Roth, A.K.L. Lim, A.P. Alivisatos, P.L. McEuen, Nature 389 (1997) 699.
[6] L. Banjai, S.W. Koch, Semiconductor Quantum Dots, World Scientific, Singapore, 1993.
[7] A. Agfeldt, M. Gratzel, Chem. Rev. 95 (1995) 49.
[8] W.P. Halperin, Rev. Mod. Phys. 58 (1986) 533.
[9] H. Weller, A. Eychmuller, Adv. Photochem. (1995) 165.
[10] S.V. Gaponenko, Optical Properties of Semiconductor Nanocrystals, Cambrige University Press, Cambridge, 1998.
[11] M.J. Sailor, J.L. Heinrich, J.M. Lauerhaas, in: P.V. Kamat, D. Meisel (Eds.), Semiconductor Nanoclusters, Studies in Surface Science and Catalysis, Vol. 103, Elsevier Science, New York, 1996, p. 209.
[12] D.A. Kondas, Report, 1993, ARFSD-TR-92024, Order No. ADA260781, 26pp.
[13] T. Hayshi, Y. Hiroshi, Jpn. Kokai Tokkyo Koho JP 02 173 (1990) 622.
[14] S.T. Lakshmikvmar, Sol. Energy. Mater. Sol. cells 32 (1994) 7.
[15] T.C. Harman, PCT Int. Appl. WO 9 416, 465; T.C. Harman, US Appl. 2 451 (1994) 12.
[16] F. Mongellaz, A. Fillot, R. Griot, J. De Lallee, Proc. SPIE-Int. Soc. Opt. Eng. 156 (1994) 2227.
[17] A.A. Korzhuev, Fiz. Khim. Orbrab. Mater. 3 (1991) 131.
[18] H.C. Metcalf, J.E. Williams, J.F. Caskta, Modern Chemistry; Holt, Reinhart, Winston, New York, 1982, p. 54.
[19] R. Coustal, J. Chim. Phys. 38 (1958) 277.
[20] C.D. Lokhande, P.S. Patil, H. Trbutsch, A. Ennaoui, Sol. Energy Mater. Sol. Cells 55 (1998) 379.
[21] M.L. Steigerwald, A.P. Alivisatos, J.M. Gibson, J. Am. Chem. Soc. 110 (1998) 3046.
[22] C.B. Murray, D.J. Norris, M.G. Bawendi, J. Am. Chem. Soc. 115 (1993) 8706.
[23] T. Rajh, O.L. Micic, A.J. Nozik, J. Phys. Chem. 97 (1993) 11999.
[24] G.S.H. Lee, D.C. Craig, I. Ma, M.L. Scudder, T.D. Bailey, I.G. Dacce, J. Am. Chem. Soc. 110 (1988) 4863.
[25] N. Herron, J.C. Calabrese, W.E. Farneth, Y. Wang, Science 259 (1993) 1426.
[26] A.L. Rogach, A. Kornowski, M.Y. Gao, A. Eychmuller, H. Weller, J. Phys. Chem. B 103 (1999) 3065.
[27] G. Henshaw, I.P. Parkin, G. Shaw, J. Chem. Soc. Chem. Commun. (1996) 1095.
[28] R.J. Bandaranayake, G.W. Wen, J.Y. Lin, H.X. Jiang, C.M. Sorensen, Appl. Phys. Lett. 67 (1995) 831.
[29] W.S. Sheldrich, M. Wachhold, Angew. Chem. Int. Ed. Engl. 36 (1997) 206.
[30] S.H. Yu, Y.S. Wu, T. Yang, Z.H. Han, Y. Xie, Y.T. Qian, X.M. Liu, Chem. Mater. 10 (1998) 2309.
[31] Z.H. Han, S.H. Yu, Y.P. Li, H.Q. Zhao, F.Q. Li, Y. Xie, Q.Y. Qian, Chem. Mater. 11 (1999) 2302.
[32] B. Li, Y. Xie, J.X. Huang, Y. Liu, Y.T. Qian, Chem. Mater. 12 (2000) 2614.
[33] J. Yang, G.H. Cheng, J.H. Zeng, S.H. Yu, X.M. Liu, Q.Y. Qian, Chem. Mater. 13 (2001) 848.
[34] W.Z. Wang, Y. Geng, B. Yan, F.Y. Liu, Y. Xie, Q.Y. Qian, J. Am. Chem. Soc. 121 (1999) 4062.
[35] Z.A. Peng, X.G. Peng, J. Am. Chem. Soc. 123 (2001) 183.
[36] J.J. Zhu, O. Palchik, S.G. Chen, A. Gedanken, J. Phys. Chem. B 104 (2000) 7344.
[37] O. Palchik, R. Kerner, A. Gedanken, A.M. Weiss, M.A. Slifkin, V. Palchik, J. Mater. Chem. 11 (2001) 874.
[38] K.S. Suslick, S.B. Choe, A.A. Cichowlas, M.W. Grimstaff, Nature 353 (1991) 414.
[39] T. Hyeon, M. Fang, K.S. Suslick, J. Am. Chem. Soc. 118 (1996) 5492.
[40] S. Avivi, Y. Mastai, G. Hodes, A. Geadnken, J. Am. Chem. Soc. 121 (1999) 4196.
[41] Y.Q. Wang, X.H. Tang, L.X.Yin.W.P. Huang, Y.R. Hacohen, A. Gedanken, Adv. Mater. 12 (2000) 1183.
[42] A.A. Kaplin, V.A. Bramin, Zh. Analit. Khim 43 (1998) 921.
[43] T.J. Mason, J.P. Walton, D.J. Lorimer, Ultrasonics 28 (1990) 333.
[44] N.A. Dhas, H. Cohen, A. Gedanken, J. Phys. Chem. B 101 (1997) 6834.
[45] M.M. Mdleleni, T. Hyeon, K.S. Suslick, J. Am. Chem. Soc. 120 (1998) 6189.
[46] Y. Mastai, R. Polsky, Y. Koltypin, A. Gedanken, G. Hodes, J. Am. Chem. Soc. 121 (1999) 10047.
[47] J.J. Zhu, S.T. Aruna, Y. Koltypin, A. Gedanken, Chem. Mater. 12 (2000) 143.
[48] J.J. Zhu, Y. Koltypin, A. Gedanken, Chem. Mater. 12 (2000) 73.
[49] H. Klug, L. Alexander (Eds.), X-ray Diffraction Procedures, Wiley, New York, 1962, p. 125.
[50] A. Guinier, X-ray Diffraction, Freeman, San Francisco, CA, 1963.
[51] T. Vossmeyer, L. Katsikas, M. Giersig, I.G. Popovic, K. Diesner, A. Chemseddine, A. Eychmuller, H. Weller, J. Phys. Chem. 98 (1994) 7665.
[52] T. Hahn, International Tables for Crystallography, D. Reidel Publishing, Boston, 1993.
[53] M.A. Malik, N. Revaprasadu, P. O'Brien, Chem. Mater. 13 (2001) 913.
[54] X1-SpecMaster System, XPS International, 1998 (Database).
[55] J.E. Bowen Katari, V.L. Colvin, A.P. Alivisatos, J. Phys. Chem. 98 (1994) 4109.
[56] Y.D. Li, H.W. Liao, Y. Ding, Y. Fan, Y. Zhang, Y.T. Qian, Inorg. Chem. 38 (1999) 1382.
[57] N. Serpone, D. Lawless, R. Khairutdinov, J. Phys. Chem. 99 (1995) 16646.
[58] J.I. Pancove, Optical Processes in Semiconductors, 1st Edition, Appendix, Dover Publication, New York, 1975.
[59] K.S. Ramaiah, R.D. Pilkington, A.E. Hill, R.D. Tomlinson, A.K. Bhatnagar, Mater. Chem. Phys. 68 (2001) 22.
[60] J. Lee, T. Tsakalakos, Nanostruct. Mater. 4 (1997) 381.
[61] K.K. Nanda, S.N. Sarangi, S. Mohanty, S.N. Sahu, Thin Solid films 322 (1998) 21.
[62] L.E. Brus, J. Phys. Chem. 90 (1986) 2555.
[63] Y. Wang, S.N. Suna, W. Mahler, R. Kosowski, J. Chem. Phys. 87 (1987) 7315.
[64] K.S. Suslick, D.A. Hammerton, R.E. Cline, J. Am. Chem. Soc. 108 (1986) 5641.
[65] K.S. Suslick, D.A. Hammerton, IEEE Trans. Ultrason. Ferroelec. Freq. Control UFFC-33 (1986) 143.
[66] T. Kondo, L.J. Kirschenbaum, H. Kim, P. Riesz, J. Phys. Chem. 97 (1993) 522.
[67] M. Gutierrez, A. Henglein, J. Pohrmann, J. Phys. Chem 91 (1987) 6687.

[68] M. Gutierrez, A. Henglein, Ch.–H. Fischer, Int. J. Radiat. Biol. 50 (1986) 313.
[69] P. Jeevanandam, Y. Koltypin, A. Gedanken, J. Mater. Chem. 10 (2000) 511.
[70] M. Ruiz, R. Ortiz, L. Perello, S. Garciagranda, M.R. Diaz, Inorg. Chim. Acta 217 (1994) 149.
[71] S. Alkaradaghi, E.S. Cedergrenzeppezauer, Z. Dauter, K.S. Wilson, Acta Crystallogr. Sect. D. Biol. Crystallogr. 51 (1995) 805.
[72] R.D. Lide, Handbook of Chemistry and Physics, Section 8, Analytical Chemistry; Vanysek, P Electrochemical Series, 81st, CRC Press, Boca Raton, FL, 2000-2001 Edition, pp. 8–21 to 8–31.
[73] K. Yasui, J. Chem. Phys. 111 (1999) 5384.